J. Phys. D: Appl. Phys. **42** (2009) 165304 (6pp) doi:10.1088/0022-3727/42/16/165304

Influence of surface morphology on sputtering yields

Qiangmin Wei[1], **Michaela Eddy**[2], **Kun-Dar Li**[1,2] **and Lumin Wang**[1,2,3]

[1] Department of Materials Science and Engineering, University of Michigan, Ann Arbor, MI 48109, USA
[2] Department of Nuclear Engineering and Radiological Science, University of Michigan, Ann Arbor, MI 48109, USA

E-mail: lmwang@umich.edu

Received 24 October 2008, in final form 30 June 2009
Published 31 July 2009
Online at stacks.iop.org/JPhysD/42/165304

Abstract
We study the variation of sputtering yields with surface morphologies under the assumption of a specially prescribed surface shape. Compared with a flat surface, we show that surface morphology can cause a decrease in the sputtering yield and an increase in the incident angle where sputtering yield is maximum. Based on Sigmund's theory, an analytical formula for the morphology dependent sputtering yield is developed by averaging the curvature dependent sputtering yield. The predicted dependence of sputtering yield on surface morphology is in good agreement with experimental observations.

(Some figures in this article are in colour only in the electronic version)

1. Introduction

Curvature dependent sputtering is a main mechanism that contributes to the evolution of surface morphologies induced by ion beam [1–7]. The understanding of this mechanism lies in the framework of Sigmund's theory [1]. For amorphous and polycrystalline materials, Sigmund proposed that the sputtering yield is proportional to the energy accumulated on the surface. By introducing discrete surface profile consisting of two intersecting planes, Sigmund found that sputtering yield is smaller on the top of a crest than on the bottom of a trough [8]. As a consequence, sharp cones appear to be more stable than flat surfaces. Extending this theory to take into account the continuum surface profile, Bradley and Harper (BH) derived a linear partial differential equation for explaining ion-induced ripple formation [2], and Cuerno and Barabási developed a nonlinear partial differential equation to interpret the evolution of ripples for a long bombardment [3]. Although Sigmund's theory focuses on the planar surface, it was shown that, under appropriate assumption of surface geometry, Sigmund's theory can be used successfully to predict surface features induced by ion beam [2, 3, 9–13]. Compared with Sigmund's theory which is based on the transport model and is valid at energies sufficiently above the threshold energy, Monte-Carlo simulation can predict sputtering behaviour in very details of energy and incidence [14]. Based on this simulation, the effects of roughness on sputtering yield have been pursued by assuming fractal surface topography and actually measured surface topography [15, 16].

Dependence of the sputtering yield on the surface curvature has been derived in the BH model. In this model, curvature dependent sputtering yield appeared in a complex differential equation in which curvature is replaced by a second derivative of surface height under small slope approximation [2]. Following this approach, the effects of morphology on sputtering yield have been investigated in recent years [17, 18]. In order to achieve analytical results, all these studies use a prescribed undulated shape of the surface. Under normal bombardment, Makeev *et al* have shown morphology effects on sputtering yield by averaging curvature dependent sputtering yield [17]. Under off-normal bombardment, no average curvature dependent sputtering yield was derived and, therefore, the derived sputtering yield is curvature dependent for a specially assumed shape rather than morphology dependent [18]. The real surface geometry is so complicated that a finite number of parameters cannot provide a full description. However, because the sign and the value of curvature change at different locations, if we assume the same amount of positive and negative curvatures, based on the previous studies, the simple equation for morphology dependent sputtering yield can be derived by averaging the

[3] Author to whom any correspondence should be addressed.

 © 2009 IOP Publishing Ltd Printed in the UK

curvature dependent sputtering yield. In this paper, we developed a formula characterizing the influence of the surface morphology on the evolution of sputtering yield. We show that surface morphologies induced by the ion bombardment can give rise to a decrease in the sputtering yield and a shift of the incident angle at which the sputtering yield is maximum.

2. Model

According to Sigmund's theory [1, 8], the sputtering yield can be expressed by

$$Y = \frac{\langle \iint_{\Re} N(\boldsymbol{r}, \varepsilon, \theta) \cdot \mathrm{d}\boldsymbol{S} \rangle}{\langle \iint_{\Re} \phi(\boldsymbol{r}) \cdot \mathrm{d}\boldsymbol{S} \rangle}, \tag{1}$$

where $N(\boldsymbol{r}, \varepsilon, \theta)$ is the number of sputtered atoms per unit area per unit time at position $\boldsymbol{r}$, ion energy ε and incident angle θ, $\phi(\boldsymbol{r})$ is the local flux of ion at $\boldsymbol{r}$, $\boldsymbol{S}$ is the surface area over the integrated range $\Re$, $\langle\rangle$ denotes the average. Here we evaluate the total number of sputtered atoms and implanted ions on a well-defined surface, and take the average over the whole area. The sputtering yield can be defined as the ratio of these two terms.

2.1. Ion energy distribution

Since the pioneering work of Bradley and Harper (BH) [2], the theory for ripple formation induced by ion beam on the surface of materials has been intensively investigated. One assumption of the BH model is the Gaussian distribution of energy which makes integration possible under small slope approximation [2, 6, 19]. According to Sigmund's theory [1], in the elastic collision region where electronic stopping is not dominant, the energy distribution $F(x)$ can be set up in terms of the moments $\langle x^n \rangle$ by the following equation:

$$F(x) = \frac{\epsilon}{\langle \Delta x^2 \rangle^{1/2}} \left[\varphi_0(\xi) - \frac{\Gamma_1}{6} \varphi_3(\xi) + \left(\frac{\Gamma_2}{24} \varphi_4(\xi) + \frac{\Gamma_1^2}{72} \varphi_6(\xi) \right) + \cdots \right], \tag{2}$$

where ϵ is the energy of ion, n is the order of moments, and

$$\langle \Delta x^n \rangle = \langle (x - \langle x \rangle)^n \rangle, \qquad n = 2, 3, \ldots, \tag{3}$$

$$\varphi_n(\xi) = \left(\mathrm{d}^n/\mathrm{d}\xi^n\right)(2\pi)^{-1/2}\,\mathrm{e}^{-\xi^2/2}, \qquad n = 0, 1, 2, \ldots, \tag{4}$$

$$\xi = (x - \langle x \rangle) / \langle \Delta x^2 \rangle^{1/2}, \tag{5}$$

$$\Gamma_1 = \langle \Delta x^3 \rangle / \langle \Delta x^2 \rangle^{3/2}, \tag{6}$$

$$\Gamma_2 = \langle \Delta x^4 \rangle / \langle \Delta x^2 \rangle^2 - 3. \tag{7}$$

Gaussian distribution is obtained by taking into account the first term in the large square brackets on the right hand side of equation (2). The corresponding coordinations are built as the x axis along the beam direction (local coordinate system). At normal bombardment under Gaussian approximation, equation (2) reduces to

$$F(r) = \frac{\epsilon}{(2\pi)^{3/2}\alpha\beta^2} \exp\left(-\frac{(x-a)^2}{2\sigma^2} - \frac{y^2 + z^2}{2\beta^2} \right), \tag{8}$$

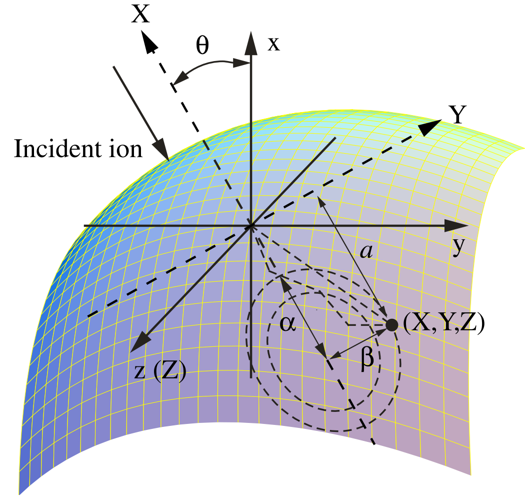

Figure 1. Schematic illustration of the two reference systems, local coordination (X, Y, Z) for ion energy distribution and laboratory frame (x, y, z) for surface profile, and the definition of projected range a and straggling α and β. The dashed curve denotes the equal energy contour.

where a is the average energy range, α and β are the stragglings of energy range along the x and y (or z) axes, respectively.

Under off-normal ion beam bombardment, it is always assumed that equation (8) does not change if the x axis is parallel to the beam direction. However, because the surface curvature is defined on another coordinate system (laboratory reference frame), there is a rotation angle (incident angle θ) between the two systems (figure 1). Coordination transformation is needed. The values in equation (2) should be derived again under the laboratory frame through the transition of the local system [1, 20]. The spatial moments for energy distribution are given by [20]

$$M_{hkm} = \int_{-\infty}^{+\infty} \int_{-\infty}^{+\infty} \int_{-\infty}^{+\infty} (\eta x' - \eta' y')^h (\eta' x' + \eta y')^k \times z^m F(x', y'z')\, \mathrm{d}x'\, \mathrm{d}y'\, \mathrm{d}z', \tag{9}$$

where $\eta = \cos\theta$, $F(x'y, z')$ is the energy distribution given by equation (8). Substituting the moments in equation (9) into equation (2), The Gaussian approximation for spatial distribution under the laboratory frame is

$$F(r) = \frac{\epsilon}{(2\pi)^{3/2}\sqrt{AB}\beta} \times \exp\left(-\frac{(x - \eta a)^2}{2A} - \frac{(y - \eta' a)^2}{2B} - \frac{z^2}{2\beta^2} \right), \tag{10}$$

where

$$A = \eta^2 \alpha^2 + \eta'^2 \beta^2, \tag{11}$$

$$B = \eta'^2 \alpha^2 + \eta^2 \beta^2. \tag{12}$$

Equation (10) gives the average energy deposited per unit volume at a point with coordinates (x, y, z) (energy density distribution) in terms of the projected range and incident angle. This equation is different from that in [17, 18]. In their approach, equation (8) was directly used and coordination transformation was performed while evaluating the surface integral.

2.2. Total sputtered atoms on a prescribed shape of surface

According to the Sigmund theory, the number of sputtered atoms per bombarding ion per area is given by

$$V(r) = \Lambda \int_{A'} \phi(r')F(r - r')\,\mathrm{d}A', \qquad (13)$$

where $\phi(\boldsymbol{r}')\,\mathrm{d}A'$ is the number of ions hitting on an area $\mathrm{d}A'$, and $\mathrm{d}A' = \sqrt{1 + (\nabla_y h')^2 + (\nabla_z h')^2}\,\mathrm{d}x'\,\mathrm{d}y'$, Λ is the materials factor [1], $\phi(\boldsymbol{r}')$ is the local flux. While evaluating the surface integral, flux as a function of surface profile is needed (local flux compared with the flux determined by equipment). For three dimensions, the simple way to calculate local flux is to use vector-valued functions. Similar to the calculation of the flow of a fluid through a surface, we can assume that both ion flux and surface have orientations. If we let the projected ion beam direction be parallel to the negative x axis (figure 1), the local flux can be represented by

$$\phi(r) = \frac{f\cos\theta}{\sqrt{1 + \nabla_y^2 x + \nabla_z^2 x}} + \frac{f\sin\theta\nabla_y x}{\sqrt{1 + \nabla_y^2 x + \nabla_z^2 x}}. \qquad (14)$$

At normal bombardment, equation (14) reduces to

$$\phi(r) = \frac{f}{\sqrt{1 + \nabla_y^2 x + \nabla_z^2 x}}. \qquad (15)$$

At off-normal bombardment for two dimensions, equation (14) reduces to

$$\phi(r) = \frac{f\cos\theta}{\sqrt{1 + \nabla_y^2 x}} + \frac{f\sin\theta\nabla_y x}{\sqrt{1 + \nabla_y^2 x}}. \qquad (16)$$

This equation is the same as that used in [2].

In the BH and extended models [2, 3, 17–19] $\boldsymbol{r} = 0$ is assumed, which means they use a special value of sputtering yield (sputtered atoms on the original point (point O in figure 1)) to describe the sputtering yield on the whole area. No average sputtering yield was performed.

In order to obtain the total sputtered atoms, we need to calculate the sputtered atoms under $\boldsymbol{r} \neq 0$. Following the approach given in the BH model [2], we assume that the surface profile is (figure 1)

$$x = -\frac{y^2}{2R_1} - \frac{z^2}{2R_2}, \qquad (17)$$

where $1/R_1$ and $1/R_2$ are the principal curvatures. Substituting equations (10), (14) and (17) into equation (13), we obtain the sputtered atom density as a function of coordinates:

$$V(r) = \left[\eta - \frac{a\eta^2}{2A^2}\left(\frac{B^2}{R_1} + \frac{\beta^2}{R_2}\right) - \frac{a\eta'^2}{R_1}\left(\frac{\eta^2 a^2}{2A^2} - 1\right) + \frac{y\eta'}{R_1}\left(1 - \frac{\eta^2 a^2}{A^2}\right)\right] fY(\theta), \qquad (18)$$

where Y_θ is the sputtering yield at incident angle θ given by $Y_\theta = \eta\Lambda\epsilon/(\sqrt{2\pi}A)\exp(-\eta^2 a^2/(2A^2))$ [21].

The total sputtered atoms as a function of curvatures and incident angle on the profile described by equation (17) can be given by the integral

$$N(R_1, R_2, \eta) = \int_A V(r)\,\mathrm{d}A. \qquad (19)$$

For a symmetrical profile with period λ, equation (19) gives

$$N(R_1, R_2, \eta) = \left[\eta - \frac{a\eta^2}{2A^2}\left(\frac{B^2}{R_1} + \frac{\beta^2}{R_2}\right) - \frac{a\eta'^2}{R_1}\left(\frac{\eta^2 a^2}{2A^2} - 1\right)\right]\lambda fY(\theta). \qquad (20)$$

2.3. Sputtering yield on a rough surface

Equation (20) describes the sputtered atoms on a specific surface with curvatures $1/R_1$ and $1/R_2$ and period λ. However, the real surface is very complex: the value and the sign of R_1 and R_2 vary and λ also varies. One possible approximation is to assume the same amount of positive and negative values of R_1 and R_2 and use average $\bar{\lambda}$. Under these assumptions, the total sputtered atoms can be

$$S = \sum_{R_1, R_2} N(R_1, R_2, \eta) \qquad (21)$$

$$= f\bar{\lambda}Y(\theta)\cos\theta. \qquad (22)$$

Because the total ion is $f\bar{\lambda}\cos\theta$, the sputtering yield at off-normal bombardment on the rough surface is $Y(\theta)$, the same as that on the flat surface. However, it is well known that sputtering yield is different for rough surfaces compared with flat surfaces. The problem is the symmetrical profile we assumed in equation (20). It was found that an asymmetrical profile can be induced by ion beam bombardment in which one side of the profile is larger than the other (figure 2) [23–25]. This asymmetrical structure can give rise to extra flux and sputtered atoms which depend on the surface morphology. Under these conditions, we need to calculate the sputtering yield again on a single surface shape and then make an average. We can assume that h varies slowly from h_1 to h_2 and corresponding y and z from $-\sqrt{2h_1 R}$ to $\sqrt{2h_2 R}$, where only radiation ions over the interval $-\sqrt{2h_1 R} \leqslant y, z \leqslant \sqrt{2h_2 R}$ have contributions to the sputtering (figure 2). The integration shows

$$Y(R, \eta) = \left[\frac{\eta - \frac{a\eta^2}{2A^2}\left(\frac{B^2}{R_1} + \frac{\beta^2}{R_2}\right) - \frac{a\eta'^2}{R_1}\left(\frac{\eta^2 a^2}{2A^2} - 1\right) + \eta'\gamma\left(1 - \frac{\eta^2 a^2}{A^2}\right)}{\eta + \gamma\eta'}\right] Y_\theta, \qquad (23)$$

where γ is a positive parameter, depending on the surface roughness, given by

$$\gamma = \sqrt{\left|\frac{h_1}{2R_1}\right|} - \sqrt{\left|\frac{h_2}{2R_1}\right|} \propto \sqrt{\left|\frac{h_0}{2R_1}\right|}, \qquad (24)$$

where h_0 can be considered as roughness height. γ is a new parameter we introduced in our model, depending on both

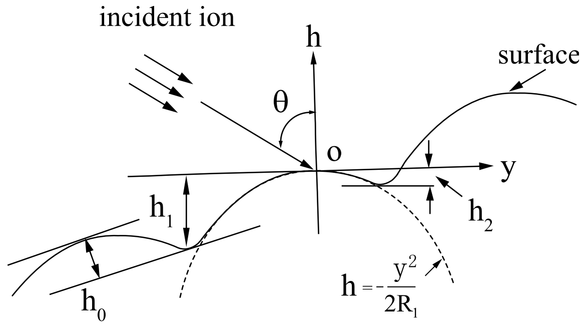

Figure 2. Side view normal to the z axis showing asymmetry profile at oblique incidence. Dashed curve shows the assumed symmetry profile given by equation (14). The integration (equation (1)) is over the range of $-\sqrt{|2h_1R_1|} \leqslant y \leqslant \sqrt{|2h_2R_1|}$.

surface roughness and curvature. No available data from theory or experiment can be obtained for γ. In order to make a comparison, the value of γ is determined by fitting the experimental data for sputtering yield after other parameters (a, α, β) are computed by simulation.

Equation (23) gives curvature dependent sputtering yield. If we assume the same amount of positive and negative curvatures in equation (23) and calculate the average sputtered atoms and average ions, respectively, the simple equation can be obtained by neglecting terms including $1/R$ in equation (23). The sputtering yield can be approximated as

$$Y(R,\theta) \approx \frac{1+\bar{\gamma}\tan\theta(1-\frac{\cos^2\theta a^2}{A^2})}{1+\bar{\gamma}\tan\theta} Y_\theta, \qquad (25)$$

where $\bar{\gamma} \propto \frac{1}{n}\sum_{i=1}^{n}\sqrt{|\frac{h_i}{2R_i}|}$, a term showing surface morphology effects on sputtering yield. Figure 3 shows the relationship between sputtering yield and incident angle given by equation (25) with different surface morphologies and energy ranges. It can be seen that the peak of sputtering yield appears around 65°–80° depending on the energy ranges and surface morphologies. The peak position of sputtering yield shifts to higher incident angles with increasing ion energy (a/α increases) or increasing surface roughness ($\bar{\gamma}$ increases). At angles smaller than 60°, the trend of sputtering yield predicted by our model is very similar to that proposed by Sigmund. At high angles, sputtering yield goes through a maximum value and then decreases dramatically to zero. These predictions are in good agreement with the experimental observations in which surface features generated by the ion bombardment can lead to a reduction in the sputtering yield [15, 16, 26–29].

2.4. Special cases

At normal bombardment, for a single surface given by equation (17), under symmetric case $\alpha = \beta$, combination of equations (1)–(10) gives

$$Y(R,0) = \left[1-\frac{a}{2}\left(\frac{1}{R_1}+\frac{1}{R_2}\right)\right]Y_0, \qquad (26)$$

where Y_0 is the sputtering yield for planar surface at normal bombardment, given by $Y_0 = \Lambda\epsilon/(\sqrt{2\pi}\alpha)\exp(-a^2/(2\alpha^2))$

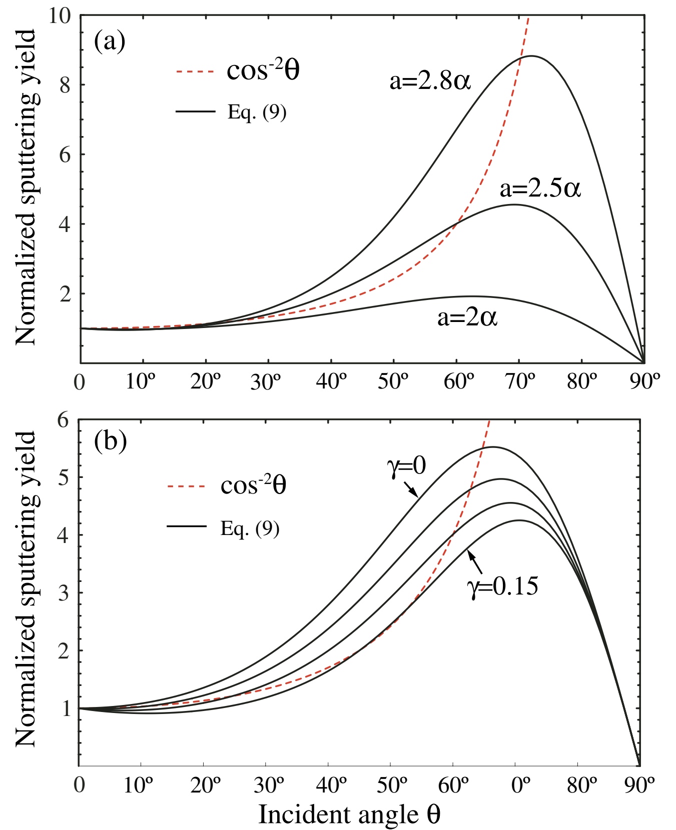

Figure 3. Angular dependence of sputtering yield given by equation (25) with (*a*) energy ranges at $\bar{\gamma} = 0.1$ and (*b*) surface morphologies at $a/\alpha = 2.5$, from top to bottom, $\bar{\gamma} = 0, 0.05, 0.1, 0.15$. Curves $(\cos^{-2}\theta)$ from Sigmund's theory are given for comparison.

[1, 8, 33]. If we replace $1/R_1$ and $1/R_2$ by the second derivatives of height in terms of y and x, under the symmetry case ($\alpha = \beta$) and normal bombardment, the same equation can be found in the BH model [2]. If we assume $R_1 = R_2 = R$, equation (26) gives the simple equation describing sputtering yield as a function of radius R:

$$Y(R,0) = \left(1-\frac{a}{R}\right)Y_0. \qquad (27)$$

This equation reveals a unique property of sputtering: the sputtering yield increases from crests (positive R) to planar surfaces ($R = \infty$) and has the maximum value for the trenches (negative R). Many features induced by ion bombardment, including ripple formation are based on this mechanism [2, 3]. For spherical particles ($R > 0$), equation (27) shows that the sputtering yield increases with increasing particle size.

3. Comparison with experiment

Figure 4 shows the comparison of angle dependent sputtering yield predicted by equation (25) with the experimental results [30–32] for different ion energies and different ion–target systems. The values of parameters used for numerical estimation of sputtering yield in equation (25) under the experimental conditions are (a) 200 keV Ar on Ni, $a = 66$ nm,

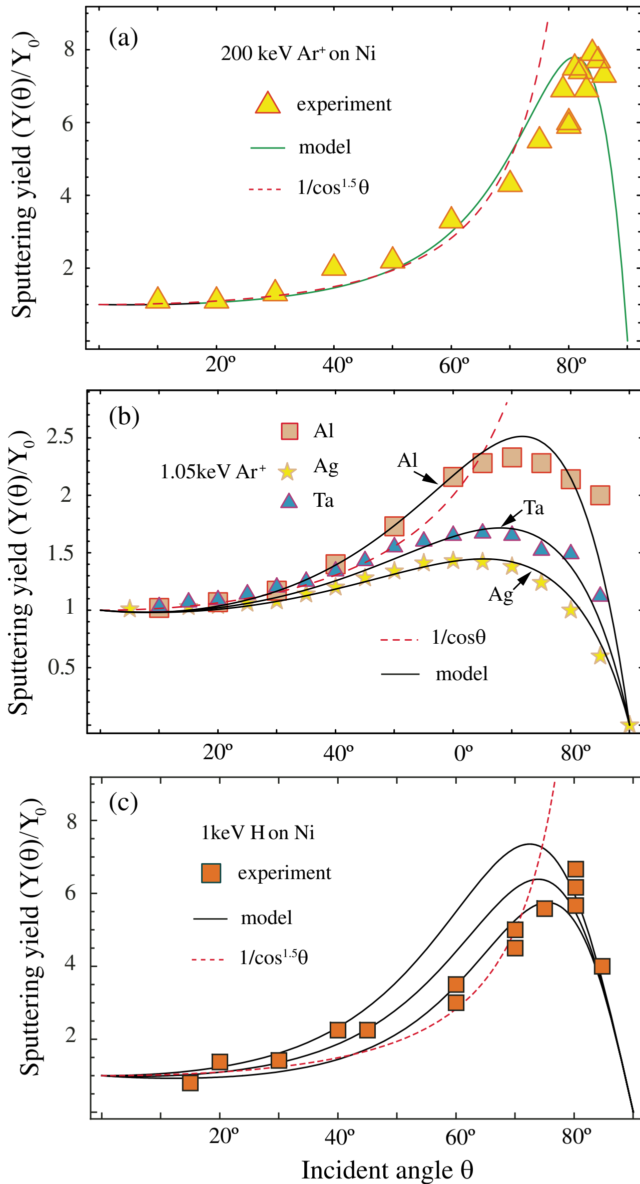

Figure 4. Comparison of angular dependence of sputtering yield predicted by the model (equation (25)) with experimental results, (*a*) 200 keV Ar ion on Ni [30], $\bar{\gamma} = 0.02$, (*b*) 1.05 keV Ar ion on Al, Ta and Ag [31], $\bar{\gamma} = 0.01$, (*c*) 1 keV H on Ni [32], from top to bottom: $\bar{\gamma} = 0, 0.05, 0.1$.

$\alpha = 25$ nm, $\beta = 11$ nm; (b) for 1.05 keV Ar on Al, $a = 2.7$ nm, $\alpha = 1.3$ nm, $\beta = 0.8$ nm, for 1.05 keV Ar on Ta, $a = 1.5$ nm, $\alpha = 0.8$ nm, $\beta = 0.6$ nm and for 1.05 keV Ar on Ag, $a = 1.5$ nm, $\alpha = 0.9$ nm, $\beta = 0.7$ nm; (c) 1 keV H on Ni, $a = 10$ nm, $\alpha = 4$ nm, $\beta = 3$ nm. We can observe that theoretical predictions in equation (25) compare fairly well with the experimental data. In figure 3(*c*), the three fitting parameters of γ are given. It can be seen that for small incident angles the morphology effects can be negligible, while at high incident angles, the morphology effects play an important role in the value and the position of maximum sputtering yield. The quantitative values of the coefficients a, α, β for energy distribution can be evaluated from the corresponding values for the ion distribution using the theory of Winterbon *et al* [34].

We use the Monte-Carlo simulation code SRIM to generate the ion distribution parameters [35].

We neglect the redeposition and shadow effects in our model. In order to get analytical resolution, small slope approximation was assumed. This condition is only valid at the beginning of bombardment where shadow and redeposition can be neglected. However, for a long bombardment, with increasing roughness and slope, these two effects should be taken into account [15].

4. Conclusions

In summary, we have introduced a continuum model for morphology dependent sputtering yield based on Sigmund's theory. For a particular surface geometry, curvature dependent sputtering yield was derived following the approach given in the BH model. In particular, we have shown that large spherical particles have higher sputtering yield than small spherical particles. For surface morphology effect, due to the asymmetric surface profile induced by the ion beam, the averaged sputtered atoms and ions which are different from the planar surface are generated and the morphology dependent sputtering yield was derived by averaging the curvature dependent sputtering yield. We found that, within the small slope approximation, with the development of surface morphology by ion bombardment, the sputtering yield decreases and the incident angle at which the sputtering yield is maximum increases. The predicted results are in reasonable accord with the experimental observations.

Acknowledgments

This work was supported by the Office of Basic Energy Science of the US Department of Energy through Grant No DE-FG02-02ER46005.

References

[1] Sigmund P 1969 *Phys. Rev.* **184** 383
[2] Bradley R and Harper J 1988 *J. Vac. Sci. Technol.* A **6** 2390
[3] Cuerno R and Barabási A-L 1995 *Phys. Rev. Lett.* **74** 4746
[4] Wei Q M, Lian J, Lu W and Wang L M 2008 *Phys. Rev. Lett.* **100** 076103
[5] Wei Q M, Li W X, Sun K, Lian J and Wang L M 2008 *J. Appl. Phys.* **103** 074306
[6] Cuenat A, George H B, Chang K C, Blakely J M and Aziz M J 2005 *Adv. Mater.* **17** 2845
[7] Gago R *et al* 2006 *Appl. Phys. Lett.* **89** 233101
[8] Sigmund P 1973 *J. Mater. Sci.* **8** 1545
[9] Bohdansky J, Roth J and Bay H L 1980 *J. Appl. Phys.* **51** 2861
[10] Yamamura Y, Matsunami N and Itoh N 1983 *Radiat. Eff.* **71** 65
[11] Matsunami N *et al* 1984 *At. Data Nucl. Data Tables* **31** 1
[12] Yamamura Y and Itoh N 1989 *Ion Beam Assisted Film Growth* (Amsterdam: Elsevier) chapter 4
[13] Bohdansky J 1984 *Nucl. Instrum. Methods Phys. Res.* B **2** 587
[14] Biersack J P and Eckstein W 1984 *Appl. Phys.* A **34** 73
[15] Küstner M, Eckstein W, Hechtl E and Roth J 1999 *J. Nucl. Mater.* **265** 22
[16] Ruzic D N 1990 *Nucl. Instrum. Methods Phys. Res.* B **47** 118
[17] Makeev M A and Barabási A-L 2004 *Nucl. Instrum. Methods Phys. Res.* B **222** 335

[18] Makeev M A and Barabási A-L 2004 *Nucl. Instrum. Methods Phys. Res.* B **222** 316
[19] Makeev M A, Cuerno R and Barabási A-L 2002 *Nucl. Instrum. Methods Phys. Res.* B **197** 185
[20] Brice D K 1975 *Ion Implantation Range and Energy Deposition Distribution* vol 1 (New York: Plenum) p 6
[21] Wei Q M, Li K D and Wang L M 2008 *J. Phys. D: Appl. Phys.* **41** 172002
[22] Carter G 1999 *J. Appl. Phys.* **85** 455
[23] Adams D P, Vasile M J, Mayer T M and Hodges V C 2003 *J. Vac. Sci. Technol.* B **21** 2334
[24] Chini T K, Okuyama F, Tanemura M and Nordlund K 2003 *Phys. Rev.* B **67** 205403
[25] Ziberi B, Frost F, Höche Th and Rauschenbach B 2005 *Phys. Rev.* B **72** 235310
[26] Stepanova M, Dew S K and Soshnikov I P 2002 *Phys. Rev.* B **66** 125407
[27] Küstner M, Eckstein W, Dose V and Roth J 1998 *Nucl. Instrum. Methods Phys. Res.* B **145** 320
[28] Wittmaack K 1990 *J. Vac. Sci. Technol.* A **8** 2246
[29] Whetten T J, Armstead A A, Grzybowski T A and Ruoff A L 1984 *J. Vac. Sci. Technol.* A **2** 477
[30] Wetz P, Krüger W, Scharmann A and Schartner K H 1997 *Radiat. Meas.* **27** 569
[31] Oechsner H 1973 *Z. Phys.* **261** 37
[32] Eckstein W 2005 *Nucl. Instrum. Methods Phys. Res.* B **232** 108
[33] Sigmund P 1981 *Sputtering by Ion Bombardment Physics and Applications* vol 1 (Berlin: Springer)
[34] Winterbon K B, Sigmund P and Sanders J B 1970 *Mat. Fys. Medd. Danske Vid. Selsk.* **37** 14
[35] Ziegler J F, Biersack J P and Littmark U 1985 *The Stopping and Range of Ions in Solid* vol 1 (Oxford: Pergamon) p 53